Optimum pyrolysis conditions to prepare the most crystalline boron carbide powder from boric acid–mannitol complex ester

Abdullah Devrim PEKDEMİR[1] ⬤, **Müşerref ÖNAL**[2,*] ⬤, **Yüksel SARIKAYA**[2] ⬤

[1]General Directorate of Mineral Research and Exploration, Ankara, Turkiye
[2]Department of Chemistry, Faculty of Science, Ankara University, Ankara, Turkiye

Abstract: A weak acidic complex ester (CE) in solid form was prepared by a condensation reaction between very weak boric acid (BA: H_3BO_3) and (D)-mannitol (MA: $C_6H_{14}O_6$) by the molar ratio of BA/MA = 2. A boron carbide (B_4C) precursor was obtained from heating of the CE at 400 °C for 4 h. The precursor was pyrolyzed under argon flow in the interval of 1300–1550 °C for 4 h and at 1400 °C for 1–4 h, respectively. The materials were examined using several techniques such as X-ray diffraction analysis, thermal analysis, scanning electron microscopy, particle size distribution, and nitrogen adsorption/desorption. The optimum pyrolysis temperature and duration were 1400 °C and 4 h, respectively. The most crystalline B_4C particles were distributed between 1 and 100 μm with a mean particle size of 20 μm. The specific surface area and specific pore volume were 13.5 $m^2 g^{-1}$ and 0.09 $cm^3 g^{-1}$, respectively. The size of the pores was between 2 and 36 nm with a mean size of 14 nm.

Key words: Boric acid, boron carbide, ester, mannitol, pyrolysis

1. Introduction

According to previous experimental studies, boron carbide (B_4C) includes many phases with different chemical composition, crystal structure, and morphology as well as their complex mixtures [1,2]. The idealized B_4C, which has a rhombohedral crystal structure, is an almost covalently bonded compound having a 6% ionic character. Some exceptional properties of B_4C are chemical inertness and low density (2.52 g mL^{-1}) and thermal expansion coefficient (5.5×10^{-6} K^{-1}) as well as high melting temperature (2450 °C), hardness (29.1 GPa), mechanical strength (350 MPa), elastic modulus (448 GPa), Seebeck coefficient (300 μV K^{-1}), and cross section (600 barns = 6×10^{-22} cm^2) for neutron absorption [3–6]. Two important disadvantages of the structure of B_4C are low fracture toughness and poor sinterability at nearly 2000 °C [7].

Due to being the third hardest material after diamond and cubic boron nitride (BN), B_4C has been used as a nonoxide ceramic for the cutting and polishing of metals and other softer ceramics [8]. Various machine parts, light mass armors for body and vehicle, protective coating of electronic surfaces, p-type semiconductors, thermocouples, diode and transistor devices, and control rods and shielding for nuclear reactors as well as materials for cancer therapy by neutron capturing have been manufactured using boron carbide and its composites [9–13]. Due to these various applications in our daily lives, various physicochemical properties have long been investigated [14–17] with ongoing detailed studies on B_4C and its composite materials [18–25].

Synthesis methods, crystal structure, and sintering of boron carbide were extensively studied [3,26]. It can be synthesized from its elements at high temperatures and pressures [27]. The methodologies used to obtain fine B_4C powder at lower temperature are safe, beneficial, and more economical than those used at higher temperature, which almost always require additional energy for heating and grinding [13,28,29]. The powder form has various morphologies including euhedral crystals, nanobelts, needle-like and elongated straight crystals, and curly clusters [3,30]. Powders having different morphologies have been synthesized from the pyrolysis of several precursors. They were obtained by the carburizing of the complex esters formed by the condensation reactions between boric acid or its derivatives and polyhydroxylated organic compounds [31–34]. These are polyols [28,35–38], saccharides [39], and polymers [40–43]. Previous studies revealed that the crystalline nature, morphology, particle size distribution, and porosity of the B_4C vary depending on the consecutive process conditions such as reactants and their molar ratio and the method used as well

---

* Correspondence: onal@science.ankara.edu.tr

1370

as pyrolysis temperature and duration. However, the optimum intervals of these variables to obtain the desirable B_4C powder have never been investigated in detail. Therefore, the objective of the present study was to determine the optimum pyrolysis conditions to obtain the most crystalline B_4C powder from the precursor of the boric acid/D-mannitol complex ester prepared at a constant molar ratio of 2.

2. Materials and methods

2.1. Boron carbide synthesis
Boric acid (BA: H_3BO_3, 99%) and D-mannitol (MA: $C_6H_{14}O_6$, 98%) were supplied by Acros Organics Ltd. (USA) and used without further purification. Because of their increasing solubility with increasing temperature of the aqueous solution of H_3BO_3 (3.0 M) and $C_6H_{14}O_6$ (3.6 M), both were prepared at 80 °C. The MA solution was slowly added to the BA solution at 80 °C with continuous stirring until it reached a molar ratio of $H_3BO_3/C_6H_{14}O_6$ = 2 [38]. This homogeneous mixture was then cooled to room temperature with constant stirring and finally left for precipitation for 24 h. The white precipitate obtained at the end of 24 h was a weak acidic complex ester (CE) formed by the condensation reaction between BA and MA. After drying at 100 °C for 4 h, the CE was granulated in an agate mortar. A precursor (PR) sample to synthesize B_4C was prepared by heating of the granular CE at 400 °C for 4 h, which were determined previously by thermogravimetric analysis. The samples taken from the PR were pyrolyzed under argon flow at various temperatures (1300, 1350, 1400, 1450, and 1500 °C) for 4 h as well as for various durations (1, 2, 3, and 5 h) at 1400 °C.

2.2. Instrumental examination
The thermogravimetric and differential thermal analysis (TG/DTA) profiles for the BA, MA, and dried CE were recorded in air between 25 and 500 °C with a heating rate of 10 K/min using a Setaram Labsys apparatus. The X-ray diffraction (XRD) patterns of the BA, MA, PR, and B_4C powders were collected using a Rigaku D-max 2200 powder diffractometer with CuK_α radiation (λ = 0.15418 nm) and a Ni filter. The scanning electron microscopy energy dispersive spectroscopy (SEM-EDS) analysis and SEM images were recorded using a FEI Quanta 400 MK2 instrument. The particle size distribution (PSD) and nitrogen adsorption/desorption isotherms (N_2-AD) at 77 K were determined for the B_4C powders synthesized by the pyrolysis. The cumulative and differential PSD curves were recorded using a Malvern Mastersizer 2000 instrument. The N_2-AD isotherms were obtained using a Quantachrome Instrument (Nova 2200 surface area and pore size analyzer). Prior to each experiment, the starting powder was outgassed under vacuum at 200 °C for 4 h.

3. Results and discussion

3.1. Thermal analysis of boric acid, mannitol, and complex ester
Thermogravimetric (TG) curves show the quantitative mass decreases in a material by heating at a constant rate of 10 K/min under air flow. The corresponding differential thermal analysis (DTA) curve represents the endothermic or exothermic nature of the heat exchanges with mass changes. The endothermic decomposition steps of BA to boron oxide (B_2O_3) are shown by 1, 2, and 3 in Figure 1a. The endothermic chemical reaction, temperature interval, and mass change percent for each step and total reaction (TR) are respectively given in the following forms:

1) $6H_3BO_3 \rightarrow 2H_3B_3O_6 + 6H_2O$,	96–163 °C,	27%
2) $2H_3B_3O_6 \rightarrow H_4B_6O_{11} + H_2O$,	163–197 °C,	5%
3) $H_4B_6O_{11} \rightarrow 3B_2O_3 + 2H_2O$,	197–350 °C,	10%
TR) $2H_3BO_3 \rightarrow B_2O_3 + 3H_2O$,	96–350 °C,	42%

Here $H_3B_3O_6$ and $H_4B_6O_{11}$ are the unstable intermediate phases. The temperature intervals and mass changes measured during the chemical reactions and evaluated from TG/DTA curves overlapped with each other, indicating that the endothermic peaks in the DTA curves correspond to the specific reactions.

The endothermic change without mass loss between 160 and 190 °C as seen in Figure 1b is due to the melting of MA. The consecutive endothermic and exothermic changes with the various mass losses between 300 and 400 °C in Figure 1b are due to the tentative thermal decomposition of MA and burning the gaseous organic products, respectively. As a result, MA completely disappears at approximately 400 °C.

Two consecutive endothermic changes with the total mass loss of 30% between 50 and 250 °C in Figure 1c arise from the melting of the CE and thermal decomposition of BA, which is left as an impurity. Furthermore, the exothermic change with 28% mass loss between 250 and 425 °C originates from the combustion of the gaseous products. The carburized CE was used as PR to prepare more crystalline B_4C powders.
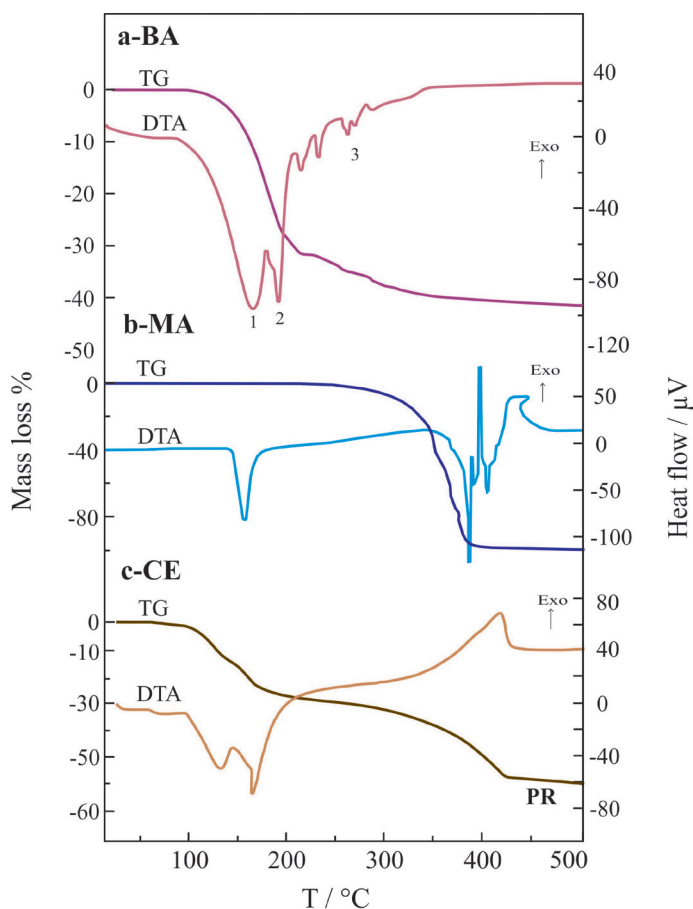
Figure 1. The TG/DTA curves of a) boric acid (BA), b) mannitol (MA), and c) complex ester (CE) containing precursor (PR) position.

3.2. XRD patterns of boric acid, mannitol, and precursor

The most intensive XRD reflection for a crystal is a characteristic feature used to distinguish it from others. Accordingly, the characteristic reflections for BA, MA, and PR located at the 2θ positions of 28.0°, 23.5°, and 21.2°, respectively, are seen in Figure 2a, 2b, and 2c. Accordingly, the PR contains a poor crystalline B_4C and impurities including C and B_2O_3.

3.3. Optimum pyrolysis conditions of the precursor

In Figures 3 and 4, the XRD patterns show the formation of crystalline B_4C powders by pyrolysis of the PR at different temperatures for 4 h and for different times at 1400 °C, respectively. The Miller indices (hkl) for the parallel crystal surfaces of B_4C are given on the corresponding peak intensities. The most intensive XRD reflection for the B_4C was located at a position of 2θ = 38.7° as seen in Figures 3 and 4 [6,28]. The crystallinity of B_4C is found to increase at least 15-fold during pyrolysis of the precursor including C and B_2O_3 impurities. Although most of the prepared B_4C powders contain B_2O_3 and C as impurities, the one obtained by 4 h pyrolysis at 1400 °C contains only B_2O_3, which was consistent with previous studies [37–40]. The present work documents that the existence and amount of elemental carbon vary depending on its pyrolysis temperature and time, as well as the chemical structure of its complex ester and precursor.

Intensity changes of the most characteristic reflection (021) of the B_4C depending on the pyrolysis temperature for 4 h as well as pyrolysis time for 1400 °C are given in Figure 5a and 5b, respectively. The crystalline feature of B_4C powders after pyrolysis for 4 h changes with temperature, reaching its maximum crystallinity at 1400 °C. Similarly, the crystallinity of B_4C powders following pyrolysis at 1400 °C changes over time, reaching its maximum crystallinity in 4 h. Accordingly, the optimum pyrolysis temperature and duration for the preparation of the most crystalline B_4C powders are 1400 °C and 4 h, respectively.

3.4. Morphology, particle size, and porosity of the most crystalline B_4C powder

In Figure 6, the SEM image of the most crystalline powder shows that the microparticles were formed through accumulation
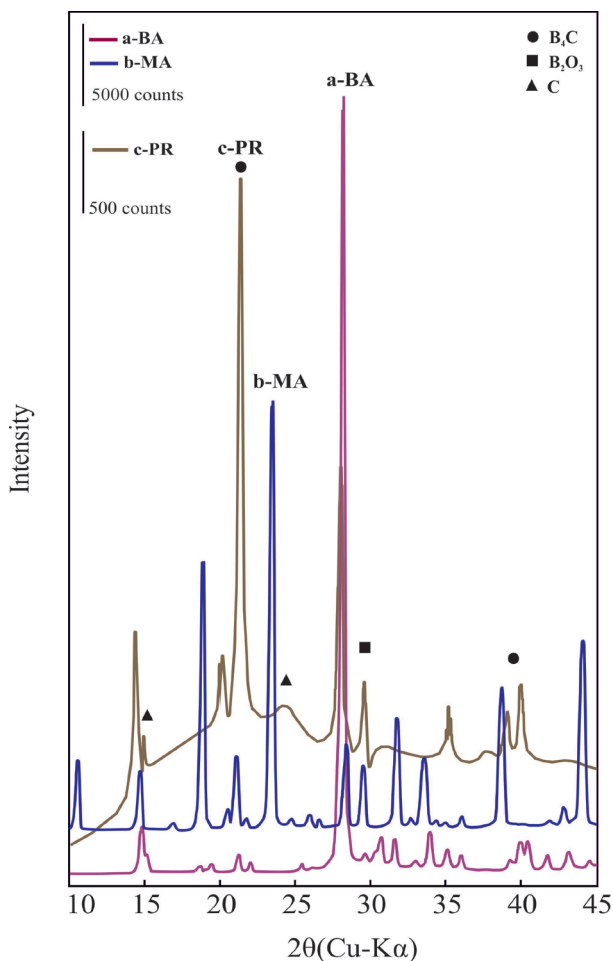
Figure 2. The XRD pattern of a) boric acid (BA), b) mannitol (MA), and c) precursor (PR), which is a heterogeneous mixture of the poor crystalline boron carbide (B_4C), boron oxide (B_2O_3), and elemental carbon (C).

of nanocrystals of B_4C. The cumulative and differential PSD curves indicate that the particle size of the same powder varies between 1 and 100 μm with a mean particle size of approximately 20 μm as seen in Figure 7.

The N_2 adsorption/desorption isotherms of the B_4C powder determined at –196 °C are given in Figure 8. Here $p/p^0 = x$ is the relative equilibrium pressure of the adsorption as the ratio of the equilibrium pressure (p) to the vapor pressure (p^0) of the liquid nitrogen. The adsorption capacity (v/cm³ g⁻¹) is defined as the volume of adsorbed gas at 0 °C and 1 atm on 1 g of adsorbent solid. Since the adsorption/desorption isotherms are convex to the p/p^0 axis over the complete range, the B_4C powder would be considered purely mesoporous adsorbent according to the IUPAC classification [44].

The mesopores filled with the liquid N_2 by capillary condensation occurred after consecutive monomolecular and multimolecular adsorptions. In contrast, capillary evaporation took place along with the desorption isotherm. Since the capillary condensation begins from the narrowest pores and capillary evaporation from the largest pores a hysteresis loop occurs between the two.

Adsorbed mass on unit mass adsorbate (m/g g⁻¹) is defined as gravimetric adsorption capacity. This quantity can be calculated from the volumetric adsorption capacity (v/cm³ g⁻¹) using the following relationship:

$$m = (v/V)\, M, \tag{1}$$

where V = 22,400 cm³ mol⁻¹ is the molar volume of gaseous N_2 at 0 °C and 1 atm, and M = 28 g mol⁻¹ is the mol mass of N_2. Using gravimetric adsorption capacity the linearized Brunauer, Emmett, and Teller (BET) equation [44] derived for multimolecular adsorption can be written in the following from:
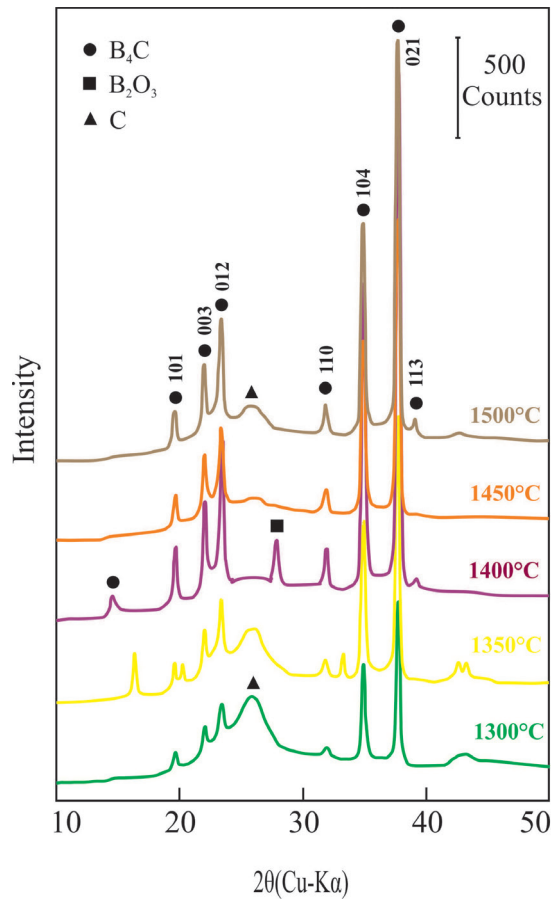
Figure 3. The XRD patterns of the B$_4$C powders pyrolyzed for 4 h at different temperatures.

$$\frac{1}{m\,(1-p/p^0)} = \frac{1}{m_m c} + \frac{(c-1)}{m_m c}\,\frac{p}{p^0},$$ (2)

where m$_m$ is monomolecular adsorption capacity and c is a constant. The BET straight line is automatically plotted according to this equation as seen in Figure 8. Surface area per unit mass adsorbent is taken as specific surface area (A/ m^2 g^{-1}). The A of the B$_4$C powder is automatically calculated using the m$_m$ value evaluated from the BET plot using the following equation:

$$A = n_m N_A \sigma_{N_2} = (m_m/M)_{N_2} N_A \sigma_{N_2},$$ (3)

where n$_m$ (mol g^{-1}) = m (g g^{-1})/28 g mol^{-1} is the material content of the monomolecular capacity, N$_A$ = 6.02 × 10^{23} mol^{-1} is the Avogadro constant, and σ_{N_2} = 6.2 × 10^{-20} m^2 is the occupied area of the molecule. The A for the B$_4$C powder calculated using these relations is A = 13.5 m^2 g^{-1}. This relatively low value also shows that the B$_4$C powder has a purely mesoporous structure.

Adsorption and desorption capacities can be also defined as liquid N$_2$ volume (V/cm^3 g^{-1}). Their values are calculated using the following relationship:

$$V = \frac{v}{22,400\ cm^3 mol^{-1}}\,V_{N_2},$$ (4)

where V_{N_2} = 34.65 cm^3 mol^{-1} is the molar volume of liquid nitrogen at –196 °C. The inner diameter (D) of pores is computed from the corrected Kelvin equation depending on the relative equilibrium pressure of the nitrogen adsorption on a solid.
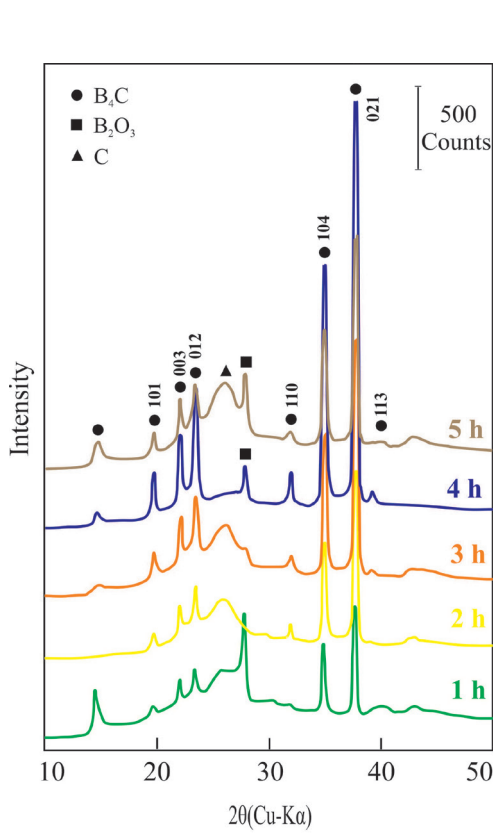
Figure 4. The XRD patterns of the B$_4$C powders pyrolyzed at 1400 °C for different times.

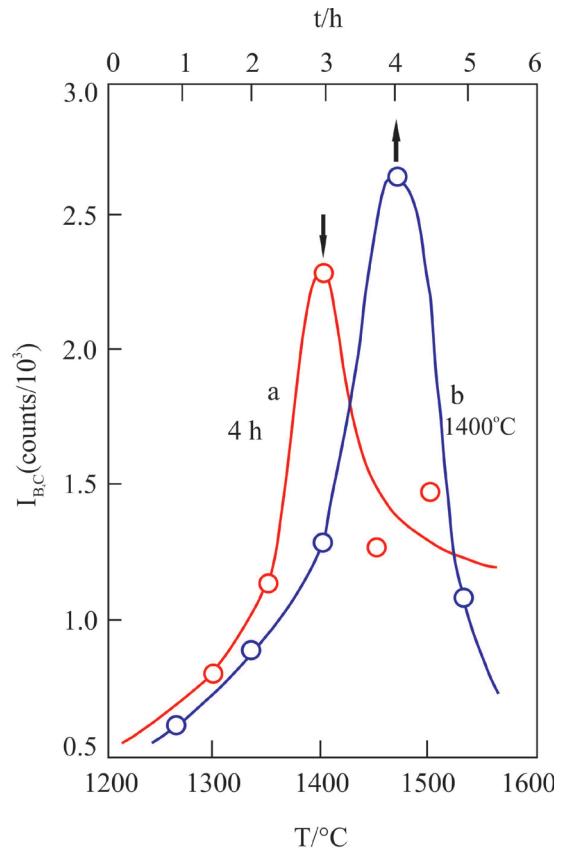**Figure 5.** Change in the crystallinity of B$_4$C powder depending on a) pyrolysis temperature for 4 h and b) pyrolysis time at 1400 °C.
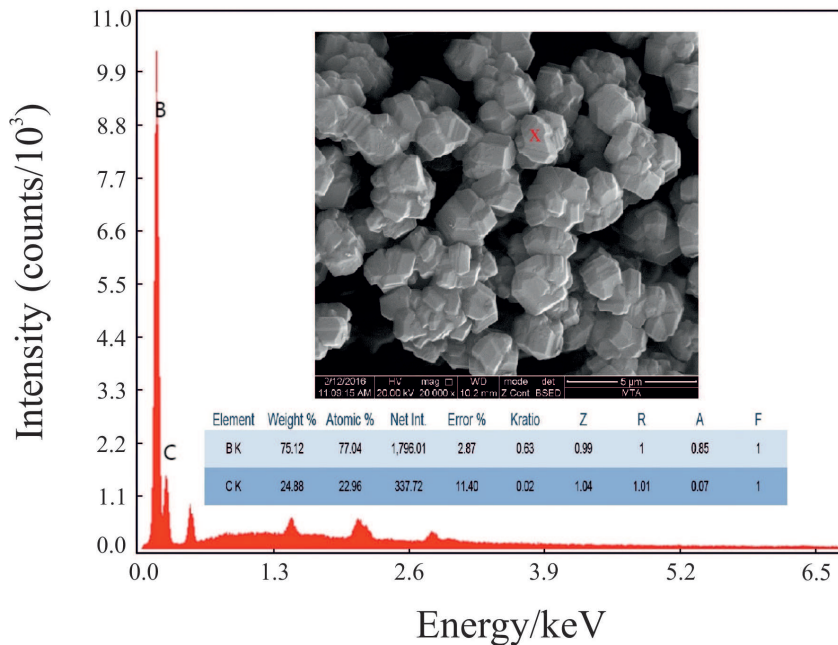

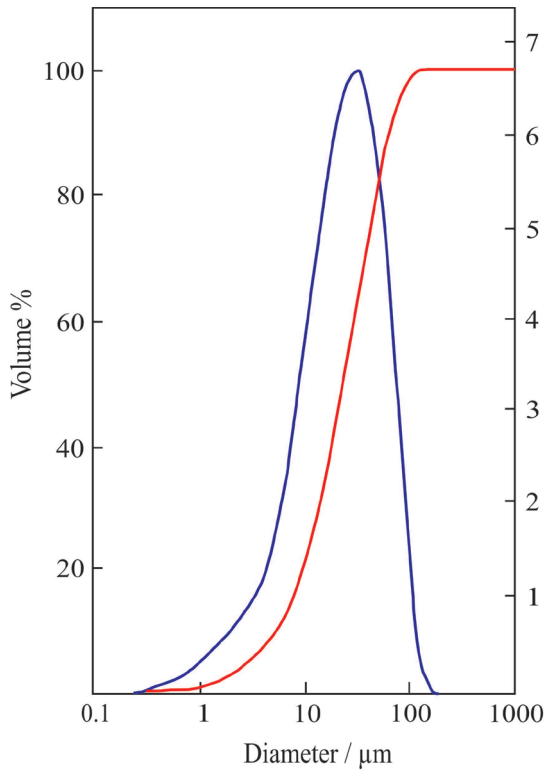**Figure 6.** SEM image and spectrum of the B$_4$C powder.

Figure 7. The cumulative and differential particle size distributions of the B₄C powder.
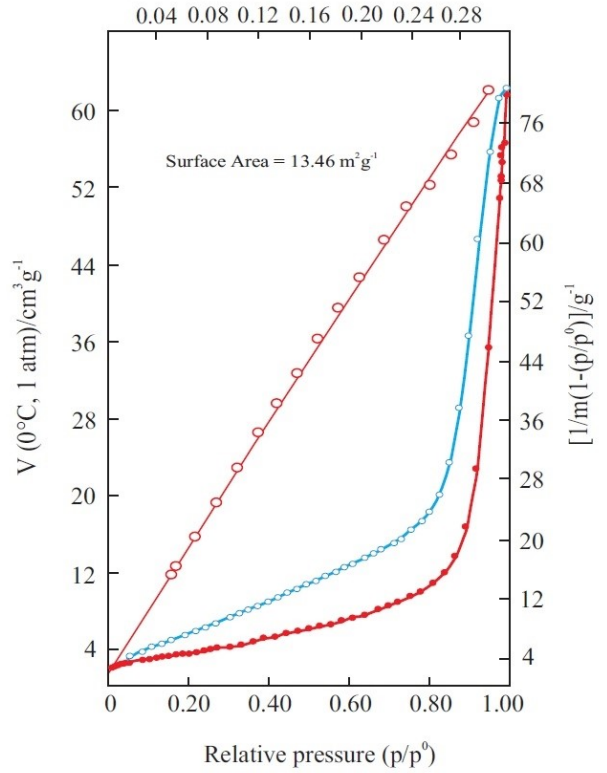

Figure 8. Nitrogen adsorption/desorption isotherms and BET straight line of the B₄C powder.
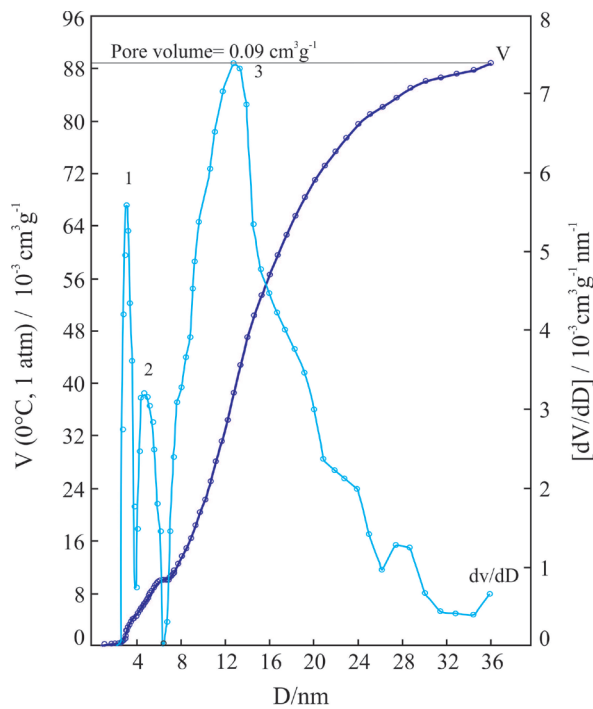

Figure 9. The cumulative and differential pore size distribution of the B₄C powder.

The cumulative pore size distribution (V-D) and differential pore size distribution (dV/dD-D) are seen in Figure 9. The maximum adsorption capacity as liquid N_2 volume reading from V-D curves is V = 0.09 $cm^3 g^{-1}$, which is specific pore volume. This low value shows that the B_4C powder is a poor mesoporous solid. There are three group mesopores with different volume and range of size as seen in Figure 9. Here the volume and size interval of the groups are respectively 1) 0.004 $cm^3 g^{-1}$, 3–4 nm; 2) 0.006 $cm^3 g^{-1}$, 4–7 nm; and 3) 0.080 $cm^3 g^{-1}$, 7–36 nm. First and second group mesopores would arise from the inner-particle voids, whereas the third group forms the largest mesopores due to intraparticle voids.

4. Conclusion

The impurity as well as the crystallinity of B_4C powders synthesized using the method described in this study vary depending on the temperature and duration of the pyrolysis application. B_2O_3 and C or only B_2O_3 are formed as impurities. It was determined that the crystallinity of B_4C powders reached its maximum when they did not contain C as an impurity. This result agrees with the data collected in previous studies. It was observed that adsorption properties such as the specific pore volume and specific surface area of B_4C powders ranging in size from 1 to 100 μm were low.

References

[1] Ponomarev VI, Kovalev ID, Konovalikhin SV, Chuev II, Vershinnikov VI et al. High temperature X-ray powder diffraction study of boron carbide crystals of different composition. Journal of Solid State Chemistry 2020; 290: 121579. https://doi.org/10.1016/j.jssc.2020.121579

[2] Watts JL, Spratt HJ, Talbot PC, Alarco JA, Raftery NA et al. Precision structural and phase analysis of boron carbide. Ceramics International 2020; 46 (8): 11033-11040. https://doi.org/10.1016/j.ceramint.2020.01.120

[3] Suri AK, Subramanian C, Sonber JK, Murthy TSRC. Synthesis and consolidation of boron carbide: a review. International Materials Reviews 2010; 55 (1): 4-40. https://doi.org/10.1179/095066009X12506721665211

[4] Carter CB, Norton MG. Ceramic Materials: Science and Engineering 2nd ed. Switzerland: Springer; 2013.

[5] Alexander R, Murthy TSRCh, Vasanthakumar K, Karthiselva NS, Bakshi SR et al. In-situ synthesis and densification of boron carbide and boron carbide-graphene nanoplatelet composite by reactive spark plasma sintering. Ceramics International 2018; 44 (17): 21132-21137. https://doi.org/10.1016/j.ceramint.2018.08.154

[6] Roumiguier L, Jankowiak A, Pradeilles N, Antou G, Maître A. Mechanical properties of submicronic and nanometric boron carbides obtained by spark plasma sintering: influence of B/C ratio and oxygen content. Ceramics International 2019; 45 (8): 9912-9918. https://doi.org/10.1016/j.ceramint.2019.02.033

[7] Sivkov A, Rakhmatullin I, Shanenkov I, Shanenkova Y. Boron carbide B_4C ceramics with enhanced physico-mechanical properties sintered from multimodal powder of plasma dynamic synthesis. International Journal of Refractory Metals and Hard Materials 2019; 78: 85-91. https://doi.org/10.1016/j.ijrmhm.2018.09.003

[8] Thévenot F. Boron carbide–a comprehensive review. Journal of European Ceramic Society 1990; 6: 205-225. https://doi.org/10.1016/0955-2219(90)90048-K

[9] Jianxin D. Erosion wear of boron carbide ceramic nozzles by abrasive air-jets. Materials Science Engineering A. 2005; 408 (1-2): 227-233. https://doi.org/10.1016/j.msea.2005.07.029

[10] Sasaki S, Takeda M, Yokoyama K, Miura T, Suzuki T et al. Thermoelectric properties of boron-carbide thin film and thin film based thermoelectric device fabricated by intense-pulsed ion beam evaporation. Science and Technology Advanced Materials 2005; 6 (2): 181-184. https://doi.org/10.1016/j.stam.2004.11.010

[11] Chen Y, Chung YW, Li SY. Boron carbide and boron carbonitride thin films as protective coatings in ultra-high density hard disk drives. Surface Coating Technology 2006; 200 (12-13): 4072-4077. https://doi.org/10.1016/j.surfcoat.2005.02.164

[12] Mortensen MW, Sørensen PG, Björkdahl O, Jensen MR, Gundersen HJG et al. Preparation and characterization of Boron carbide nanoparticles for use as a novel agent in T cell-guided boron neutron capture therapy. Applied Radiation and Isotopes 2006; 64 (3): 315-324. https://doi.org/10.1016/j.apradiso.2005.08.003

[13] Li J, Cao K, Li J, Liu M, Zhang S et al. Synthesis and ceramic conversion of a new organodecaborane preceramic polymer with high-ceramic-yield. Molecules 2018; 23 (10): 2461. https://doi.org/10.3390/molecules23102461

[14] Jain A, Anthonysamy S. Oxidation of boron carbide powder. Journal of Thermal Analysis and Calorimetry 2015; 122 (2): 645-652. https://doi.org/10.1007/s10973-015-4818-3

[15] Liang D, Liu J, Li H, Zhou Y, Zhou J. Improving effect of boron carbide on the combustion and thermal oxidation characteristics of amorphous boron. Journal of Thermal Analysis and Calorimetry 2017; 128 (3): 1771-1782. https://doi.org/10.1007/s10973-016-5989-2

[16] Arumugachamy A, Lakshmana Pandian P, Kadarkaraithangam J. Study of thermal and safety behaviour of nanoboron blended flash powder Journal of Thermal Analysis and Calorimetry 2021; 146 (1): 483-491. https://doi.org/10.1007/s10973-021-10891-3

[17] Kozekanan BS, Moradkhani A, Baharvandi H, Ehsani N. Thermodynamic and phase analysis of SiC-nano/microB$_4$C-C composites produced by pressureless sintering method. Journal of the Korean Ceramic Society 2022; 59: 180-192. https://doi.org/10.1007/s43207-021-00173-x

[18] Kozień D, Jeleń P, Stępień J, Olejniczak Z, Sitarz M et al. Surface properties and morphology of boron carbide nanopowders obtained by lyophilization of saccharide precursors. Materials 2021; 14: 3419. https://doi.org/10.3390/ma14123419

[19] Ugraskan V, Isik B, Yazici O, Cakar F. Surface characterization and synthesis of boron carbide and silicon carbide. Solid State Sciences 2021; 118: 106636. https://doi.org/10.1016/j.solidstatesciences.2021.106636

[20] Zakaryan MK, Zurnachyan AR, Amirkhanyan NH, Kirakosyan HV, Antonov M et al. Novel pathway for the combustion synthesis and consolidation of boron carbide. Materials 2022; 15: 5042. https://doi.org/10.3390/ma15145042

[21] Song Q, Zhang ZH. Microstructure and self-healing mechanism of B$_4$C–TiB$_2$–SiC composite ceramic after pre-oxidation behavior. Ceramics International 2022; 48: 25458-25464. https://doi.org/10.1016/j.ceramint.2022.05.223

[22] Koysuren O, Koysuren HN. Preparation and activity evaluation of B$_4$C/ZnO composite photocatalyst. Journal of Sol-Gel Science and Technology 2022; 103: 172-184. https://doi.org/10.1007/s10971-022-05797-x

[23] Coban O, Bugdayci M, Acma ME. Production of B$_4$C-TiB$_2$ composite powder by self-propagating high-temperature synthesis. Journal of the Australian Ceramic Society 2022; 58: 777-791. https://doi.org/10.1007/s41779-022-00714-5

[24] Povlov IS, Ivanova AG, Filonenko VP, Zibrov I P, Voloshin AE et al. The rhombic hexecontahedron boron carbide microcrystals – crystal structure analysis. Scripta Materialia 2023; 222: 115023. https://doi.org/10.1016/j.scriptamat.2022.115023

[25] Koysuren O, Koysuren HN. Synthesis of B$_4$C powder via the carbothermal reduction and photoreduction of Cr(VI) on B$_4$C under visible light irradiation. Journal of the Korean Ceramic Society 2023; 60: 798-810. https://doi.org/10.1007/s43207-023-00307-3

[26] Swapna MS, Saritha Devi MS, Sankararaman S. Boron-rich boron carbide from soot: a low-temperature green synthesis approach. Journal of the Korean Ceramic Society 2020; 57: 651-657. https://doi.org/10.1007/s43207-020-00066-5

[27] Chakraborti A, Vast N, Le Godec Y. Synthesis of boron carbide from its elements at high pressures and high temperatures. Solid State Sciences 2020; 104: 106265. https://doi.org/10.1016/j.solidstatesciences.2020.106265

[28] Kakiage M, Ohashi T, Shiomi S, Kobayashi H. Morphological changes of calcium hexaboride powder synthesized from condensed boric acid-polyol product. Advanced Powder Technology 2019; 30 (3): 644-648. https://doi.org/10.1016/j.apt.2018.12.016

[29] Gao S, Li X, Wang S, Xing P, Kong J et al. A low cost, low energy, environmentally friendly process for producing high-purity boron carbide. Ceramics International 2019; 45 (3): 3101-3110. https://doi.org/10.1016/j.ceramint.2018.10.202

[30] Avcioglu S, Kaya F, Kaya C. Non-catalytic synthesis of boron carbide (B$_4$C) nano structures with various morphologies by sol-gel process. Materials Letters 2019; 249: 201-205. https://doi.org/10.1016/j.matlet.2019.04.056

[31] Avcioglu S, Kaya F, Kaya C. Morphological evolution of boron carbide particles: sol-gel synthesis of nano/micro B$_4$C fibers. Ceramics International 2021; 47: 26651-26667. https://doi.org/10.1016/j.ceramint.2021.06.073

[32] Karaahmet O, Cicek B, Effect of mechanically modification process on boron carbide synthesis from polymeric precursor method. Ceramics International 2022; 48: 11940-11952. https://doi.org/10.1016/j.ceramint.2022.01.043

[33] Springsteen G, Wang B. A detailed examination of boronic acid–diol complexation. Tetrahedron 2002; 58 (26): 5291-5300. https://doi.org/10.1016/S00404020(02)00489-1

[34] Shvarts EM, Ignash RT, Belousova RG. Reactions of polyols with boric acid and sodium monoborate. Russian Journal of General Chemistry 2005; 75 (11): 1687-1692. https://doi.org/10.1007/s11176-005-0492-7

[35] Peters JA. Interactions between boric acid derivatives and saccharides in aqueous media: structures and stabilities of resulting esters. Coordination Chemistry Review 2014; 268: 1-22. https://doi.org/10.1016/j.ccr.2014.01.016

[36] Lopalco A, Stella VJ, Thompson WH. Origins, and formulation implications, of the pK difference between boronic acids and their esters: a density functional theory study. European Journal of Pharmaceutical Sciences 2018; 124: 10-16. https://doi.org/ 10.1016/j.ejps.2018.08.017

[37] Kakiage M, Tahara N, Yanase I, Kobayashi H. Low-temperature synthesis of boron carbide powder from condensed boric acid–glycerin product. Materials Letters 2011; 65 (12): 1839-1841. https://doi.org/10.1016/j.matlet.2011.03.046

[38] Kakiage M, Tominaga Y, Yanase I, Kobayashi H. Synthesis of boron carbide powder in relation to composition and structural homogeneity of precursor using condensed boric acid–polyol product. Powder Technology 2012; 221: 257-263. https://doi.org/10.1016/j.powtec.2012.01.010

[39] Tahara N, Kakiage M, Yanase I, Kobayashi H. Effect of addition of tartaric acid on synthesis of boron carbide powder from condensed boric acid–glycerin product. Journal of Alloys and Compounds 2013; 573: 58-64. https://doi.org/10.1016/j.jallcom.2013.03.255

[40] Fathi A, Ehsani N, Rashidzadeh M, Baharvandi H, Rahimnejad A. Synthesis of boron carbide nano particles using polyvinyl alcohol and boric acid. Ceramic-Silikaty 2012; 56 (1): 32-35.

[41] Kozień D, Jeleń P, Sitarz M, Bućko MM. Synthesis of boron carbide powders from mono- and polysaccharides. International Journal of Refractory Metals and Hard Materials 2020; 86: 105099. https://doi.org/10.1016/j.ijrmhm.2019.105099

[42] Shawgi N, Li S, Wang S. A novel method of synthesis of high purity nano plated boron carbide powder by a solid-state reaction of poly (vinyl alcohol) and boric acid. Ceramics International 2017; 43 (13): 10554-10558 https://doi.org/10.1016/j.ceramint.2017.05.120

[43] Wang J, Gou Y, Zhang Q, Jian K, Chen Z et al. Linear organodecaborane block copolymer as a single-source precursor for porous boron carbide ceramics. Journal of European Ceramic Society 2017; 37 (5): 1937-1943. https://doi.org/10.1016/j.jeurceramsoc.2016.12.035

[44] Rouquerol F, Rouquerol J, Sing KSW, Llewellyn P, Maurin G. Adsorption by Powders and Porous Solids. 2nd ed. Amsterdam, Netherlands: Academic Press; 2014.